https://doi.org/10.15407/ujpe63.10.881

M. AYGUN

Department of Physics, Bitlis Eren University
(Bitlis, Turkey; e-mail: murata.25@gmail.com)

A COMPARISON OF PROXIMITY POTENTIALS IN THE ANALYSIS OF HEAVY-ION ELASTIC CROSS SECTIONS

To obtain alternative nuclear potentials is very important in explaining the heavy-ion reactions, as well as light-ion ones. For this purpose, a comprehensive analysis of six different proximity potentials ([1, 9–12, 15]) is performed for the first time in the present study. In order to see the availability of the potentials, the elastic-scattering angular distributions of ^{40}Ca by different target nuclei from ^{32}S to ^{208}Pb are calculated within the framework of the optical model. The theoretical results are compared with each other and with experimental data. The similarities and differences of the potentials are discussed, and some alternative potentials are proposed.

K e y w o r d s: nuclear potentials, proximity potentials, elastic scattering.

1. Introduction

^{40}Ca is an important nucleus for heavy-ion elastic scattering reactions in the field of nuclear physics. In this context, the results of studies of the elastic scattering of the ^{40}Ca projectile by different target nuclei can be found from the literature. For example, the elastic scattering in the $^{40}\mathrm{Ca} + {}^{32}\mathrm{S}$ reaction at 100 MeV has been measured by Baeza *et al.* [2]. They have analyzed the experimental data by using the double folding model and have stated the necessity of a renormalization factor equal to 1.57. The elastic scattering data for the $^{40}\mathrm{Ca} + {}^{40}\mathrm{Ca}$ system have been measured at various incident energies [3]. Doubre *et al.* [3] have explained the difficulty of the theoretical analysis of the scattering of ^{40}Ca nuclei on ^{40}Ca. The scattering cross-sections for the $^{40}\mathrm{Ca} + {}^{90}\mathrm{Zr}$ reaction at 139.8, 150.7, and 152 MeV and the $^{40}\mathrm{Ca} + {}^{96}\mathrm{Zr}$ reaction at 133.8, 135.5, 150.4, and 152 MeV have been measured in [4,5]. The elastic scattering cross-section of ^{40}Ca on ^{208}Pb at 302 MeV has been reported in Ref. [6]. In the general meaning, the theoretical analysis of these experimental data have been performed by using the Woods–Saxon or double folding potentials. On the other hand, the detection of potential parameters for heavy-ions is difficult due to the strong absorption and is not certain [7]. If the number of free parameters of the selected potentials in the theoretical analysis increases, the theoretical analysis becomes more difficult. Sometimes, the difficulty in the analysis is that few potentials were used. In other words, it is very important to determine the appropriate potential that defines the nuclear reaction. Therefore, obtaining the alternative nuclear potentials is very important to explain heavy-ion reactions, as well as light-ion ones.

In the present study, we examine the availability of six different proximity potentials such as Broglia and Winther 1991 (BW 91) [8], Aage Winther (AW 95) [9], Bass 1980 (Bass 80) [8], Christensen and Winther 1976 (CW 76) [10], Ngô 1980 (Ngo 80) [11], and Proximity 1988 (Prox 88) [12] in explaining the elastic cross sections. With this goal, we reanalyze the elastic-scattering angular distributions of ^{40}Ca projectile by ^{32}S, ^{40}Ca, ^{90}Zr, ^{96}Zr, and ^{208}Pb target nuclei at various energies. We compare the theoretical results with the experimental data and show similarities and differences of the potentials investigated with this work.

The next section gives the information about the method and nuclear potentials used in the theoretical calculations. Section 3 displays the results and discussions. Finally, Section 4 is attributed to the summary.

2. Theoretical Formalism

2.1. Optical model

We use the optical model, which is one of the most efficient and successful models in explaining the elastic-

scattering cross-section. To obtain the real part of the optical potential, six different proximity potentials are evaluated, and each of the nuclear potentials is described in the following subsection. However, the imaginary part of the optical potential is assumed as the Woods–Saxon potential in all calculations, which is given by

$$W(r) = \frac{W_0}{\left[1+\exp\left(\frac{r-R_w}{a_w}\right)\right]}. \quad (1)$$

The code FRESCO is applied in the optical model calculations [13].

2.2. Nuclear potentials

2.2.1 Broglia and Winther 1991 (BW 91) potential

Broglia and Winther 1991 (BW 91) potential [8, 14] is assumed as

$$V_N^{\mathrm{BW\,91}}(r) = -\frac{V_0}{\left[1+\exp\left(\frac{r-R_0}{a}\right)\right]} \text{ MeV}, \quad (2)$$

where

$$V_0 = 16\pi\frac{R_1R_2}{R_1+R_2}\gamma a, \quad a = 0.63 \text{ fm}, \quad (3)$$

and

$$R_0 = R_1 + R_2 + 0.29, \quad (4)$$

$$R_i = 1.233A_i^{1/3} - 0.98A_i^{-1/3} \quad (i=1,2), \quad (5)$$

with the surface energy constant γ

$$\gamma = \gamma_0\left[1 - k_s\left(\frac{N_p-Z_p}{A_p}\right)\left(\frac{N_t-Z_t}{A_t}\right)\right], \quad (6)$$

γ_0 and k_s are 0.95 MeV/fm^2 and 1.8, respectively.

2.2.2. Aage Winther (AW 95) potential

Aage Winther (AW 95) potential is the same as BW 91 potential except for [9, 14]

$$a = \left[\frac{1}{1.17(1+0.53(A_1^{-1/3}+A_2^{-1/3}))}\right] \text{fm}, \quad (7)$$

and

$$R_0 = R_1 + R_2, \quad R_i = 1.2A_i^{1/3} - 0.09 \quad (i=1,2). \quad (8)$$

2.2.3. Bass 1980 (Bass 80) potential

Bass 1980 (Bass 80) potential evaluated in theoretical calculations is exhibited by [8, 14, 15]

$$V_N^{\mathrm{Bass\,80}}(s) = -\frac{R_1R_2}{R_1+R_2}\phi(s = r-R_1-R_2) \text{ MeV}. \quad (9)$$

The universal function $\phi(s = r - R_1 - R_2)$ is produced by [8, 14]

$$\phi(s) = \left[0.033\exp\left(\frac{s}{3.5}\right) + 0.007\exp\left(\frac{s}{0.65}\right)\right]^{-1}, \quad (10)$$

and

$$R_i = R_s\left(1 - \frac{0.98}{R_s^2}\right), \quad (11)$$

$$R_s = 1.28A_i^{1/3} - 0.76 + 0.8A_i^{-1/3} \text{ fm} \quad (i=1,2). \quad (12)$$

2.2.4. Christensen and Winther 1976 (CW 76) potential

The other proximity potential investigated in our study is Christensen and Winther 1976 (CW 76) presented by [10, 16]

$$V_N^{\mathrm{CW\,76}}(r) = -50\frac{R_1R_2}{R_1+R_2}\phi(r-R_1-R_2) \text{ MeV}, \quad (13)$$

where

$$R_i = 1.233A_i^{1/3} - 0.978A_i^{-1/3} \text{ fm} \quad (i=1,2). \quad (14)$$

The universal function $\phi(s = r - R_1 - R_2)$ is

$$\phi(s) = \exp\left(-\frac{r-R_1-R_2}{0.63}\right). \quad (15)$$

2.2.5. Ngô 1980 (Ngo 80) potential

Another potential used to determine the real potential is Ngô 1980 (Ngo 80) potential written as [11]

$$V_N^{\mathrm{Ngo\,88}}(r) = \overline{R}\phi(r-C_1-C_2) \text{ MeV} \quad (16)$$

$$\overline{R} = \frac{C_1C_2}{C_1+C_2}, \quad C_i = R_i\left[1-\left(\frac{b}{R_i}\right)^2 + ...\right], \quad (17)$$

$$R_i = \frac{NR_{ni}+ZR_{pi}}{A_i} \quad (i=1,2), \quad (18)$$

$$R_{pi} = r_{0pi}A_i^{1/3}, R_{ni} = r_{0ni}A_i^{1/3}, \quad (19)$$

$$r_{0pi} = 1.128 \text{ fm}, \ r_{0ni} = 1.1375 + 1.875\times10^{-4}A_i \text{ fm}. \quad (20)$$

The universal function $\phi(s = r - C_1 - C_2)$ (in MeV/fm) is formulated as

$$\Phi(s) = \begin{cases} -33 + 5.4(s - s_0)^2 & \text{for } s < s_0, \\ -33 \exp\left[-\frac{1}{5}(s - s_0)^2\right] & \text{for } s \geq s_0, \\ s_0 = -1.6 \text{ fm}. \end{cases}$$

2.2.6. Proximity 1988 (Prox 88) potential

Proximity 1977 (Prox 77) potential [12, 16] is given by

$$V_N^{\text{Prox}\,77}(r) = 4\pi\gamma b\overline{R}\Phi\left(\zeta = \frac{r - C_1 - C_2}{b}\right) \text{ MeV}, \quad (21)$$

$$\overline{R} = \frac{C_1 C_2}{C_1 + C_2}, \quad C_i = R_i\left[1 - \left(\frac{b}{R_i}\right)^2 + ...\right], \quad (22)$$

$$R_i = 1.28A_i^{1/3} - 0.76 + 0.8A_i^{-1/3} \text{ fm} \quad (i = 1, 2); \quad (23)$$

γ, the surface energy coefficient, is

$$\gamma = \gamma_0\left[1 - k_s\left(\frac{N - Z}{N + Z}\right)^2\right], \quad (24)$$

where $N(Z)$ is the total number of neutrons (protons). The universal function, $\Phi(\zeta)$, is given by

$$\Phi(\zeta) = \begin{cases} -\frac{1}{2}(\zeta - 2.54)^2 - 0.0852(\zeta - 2.54)^3 \\ \text{for } \zeta \leq 1.2511, \\ -3.437 \exp\left(-\frac{\zeta}{0.75}\right) \quad \text{for } \zeta \geq 1.2511. \end{cases}$$

For the Proximity 1988 (Prox 88) potential, $\gamma_0 = 1.2496$ MeV/fm^2 and $k_s = 2.3$ [8]. The other parameters of the Prox 88 potential are the same as for the Prox 77 potential.

3. Results and Discussion

We have investigated the effect of proximity potentials on the elastic-scattering cross-sections of a ^{40}Ca projectile from ^{32}S, ^{40}Ca, ^{90}Zr, ^{96}Zr, and ^{208}Pb target nuclei. The real parts of the optical potentials have been determined by using six different proximity potentials such as BW 91, AW 95, Bass 80, CW 76, Ngo 80, and Prox 88. The distance-dependent changes of the real potentials for each reaction have been shown in Fig. 1. On the other hand, the imaginary potential has been taken as the Woods–Saxon potential. While the depth (W_0), radius (r_w), and diffusion (a_w) parameters of the imaginary potential are determined, the most suitable values, which provide agreement of the results with the experimental data, have been researched. In this context, the r_w value is 1.40 fm for the ^{40}Ca + ^{32}S reaction, 1.38 fm for all the energies of the ^{40}Ca + ^{40}Ca, ^{40}Ca + ^{90}Zr, and ^{40}Ca + ^{96}Zr reactions and 1.33 fm for the ^{40}Ca + ^{208}Pb reaction. The a_w value is 0.87 fm for AW 95 potential and 0.86 fm for the other potentials of the ^{40}Ca + ^{32}S reaction, 0.35 fm for all the energies of the ^{40}Ca + ^{40}Ca reaction, 0.35 fm at 139.8 MeV and 0.50 fm for the other energies of the ^{40}Ca + ^{90}Zr reaction, 0.50 fm for all the energies of the ^{40}Ca + ^{96}Zr and 0.30 fm for the ^{40}Ca + ^{208}Pb reaction. The W_0 values have been listed in Table.

In Fig. 2, we have presented the elastic scattering results of the ^{40}Ca + ^{32}S reaction at an incident energy of 100 MeV with proximity potentials. We have observed that our results are in good agreement with the experimental data at small and large angles. However, the theoretical results miss middle angles of the experimental data. When all the theoretical results are compared with each other, it has been seen that the behaviors of our results are very similar to each other.

W_0 (MeV) values for BW 91, AW 95, Bass 80, CW 76, Ngo 80, and Prox 88 potentials used in the analysis of the ^{40}Ca + ^{32}S, ^{40}Ca + ^{40}Ca, ^{40}Ca + ^{90}Zr, ^{40}Ca + ^{96}Zr, and ^{40}Ca + ^{208}Pb systems

		W_0					
Target nucleus	Energy (MeV)	BW 91	AW 95	Bass 80	CW 76	Ngo 80	Prox 88
^{32}S	100	57.0	57.0	56.9	57.0	58.5	55.5
	176	4.70	5.00	5.70	9.80	2.10	3.70
^{40}Ca	186	3.00	3.10	4.80	9.50	4.10	3.10
	225	4.90	4.90	6.20	12.0	4.00	5.60
	240	49.0	55.0	50.0	66.1	64.0	45.0
	139.8	52.0	50.0	52.0	52.0	50.0	49.0
^{90}Zr	150.7	66.0	70.0	64.0	64.0	62.0	66.0
	152	56.0	56.0	54.0	56.0	61.0	57.0
	133.8	33.0	33.0	33.0	33.0	34.0	32.0
^{96}Zr	135.5	20.0	20.0	20.0	20.0	22.0	20.0
	150.4	93.0	99.0	90.0	93.0	106.0	93.0
	152	67.0	71.0	64.0	67.0	79.0	68.0
^{208}Pb	302	25.0	34.0	30.0	30.0	90.0	30.0

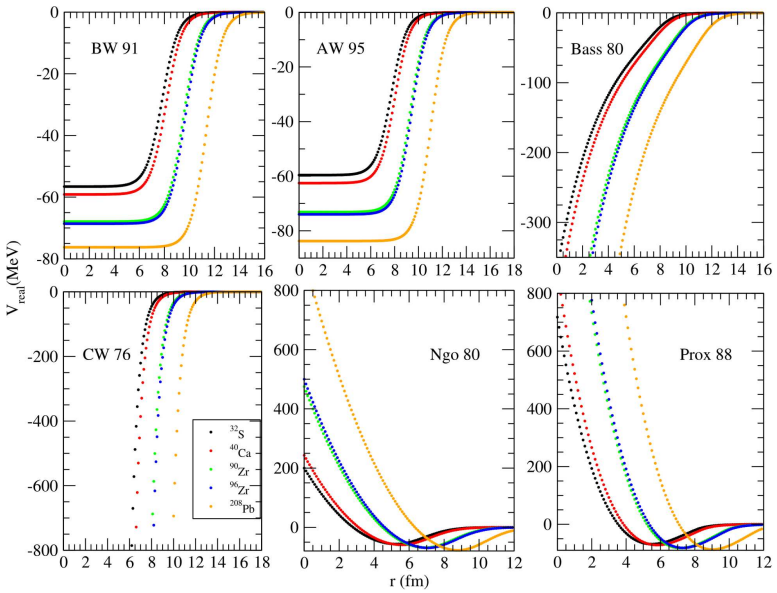

Fig. 1. Distance-dependent changes of BW 91, AW 95, Bass 80, CW 76, Ngo 80, and Prox 88 potentials for the $^{40}Ca + {}^{32}S$, $^{40}Ca + {}^{40}Ca$, $^{40}Ca + {}^{90}Zr$, $^{40}Ca + {}^{96}Zr$, and $^{40}Ca + {}^{208}Pb$ reactions

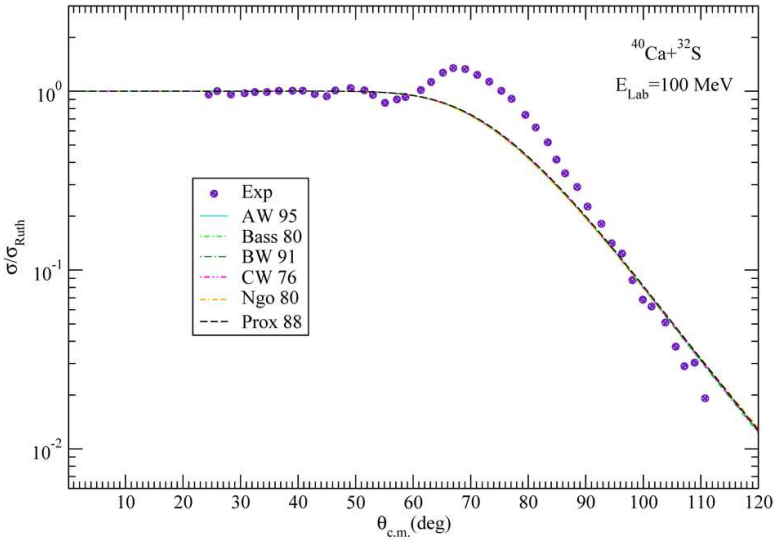

Fig. 2. The cross-sections of the $^{40}Ca + {}^{32}S$ elastic scattering in comparison with the experimental data at $E_{\rm lab} = 100$ MeV, by using AW 95, Bass 80, BW 91, CW 76, Ngo 80, and Prox 88 potentials. The experimental data have been taken from [2]

The angular distributions of elastic scattering of a ^{40}Ca projectile on ^{40}Ca target nucleus at 176, 186, 225, and 240 MeV have been shown in Fig. 3. At 176 MeV, the results of AW 95 potential are very good at describing the overall of the experimental data and are better than the results for other potentials. For 186 MeV, the AW 95 and Bass 80 results are very close to each other. However, it has been observed that the AW 95 results are in better agreement with the data than the results of all the potentials. At 225 MeV,

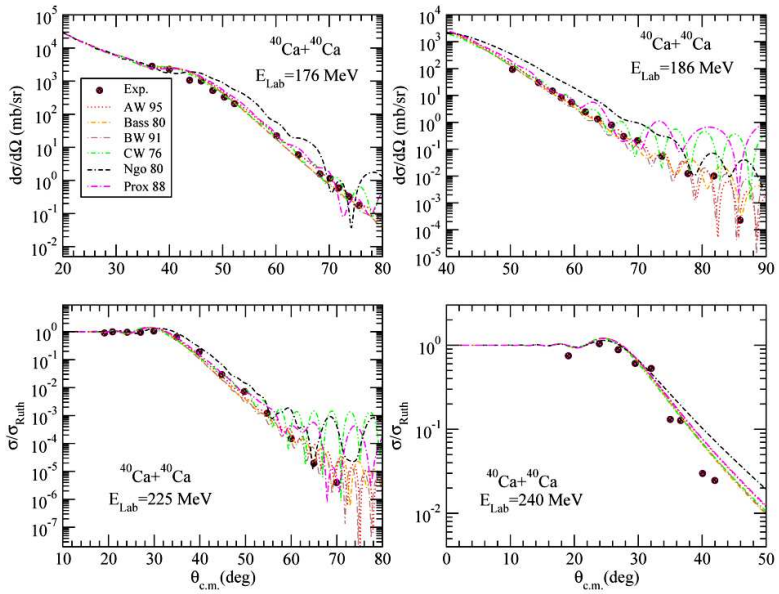

Fig. 3. The same as Fig. 2, but for the $^{40}\mathrm{Ca} + {}^{40}\mathrm{Ca}$ reaction at $E_{\mathrm{lab}} = 176$, 186, 225, and 240 MeV. The experimental data have been taken from [3, 7]

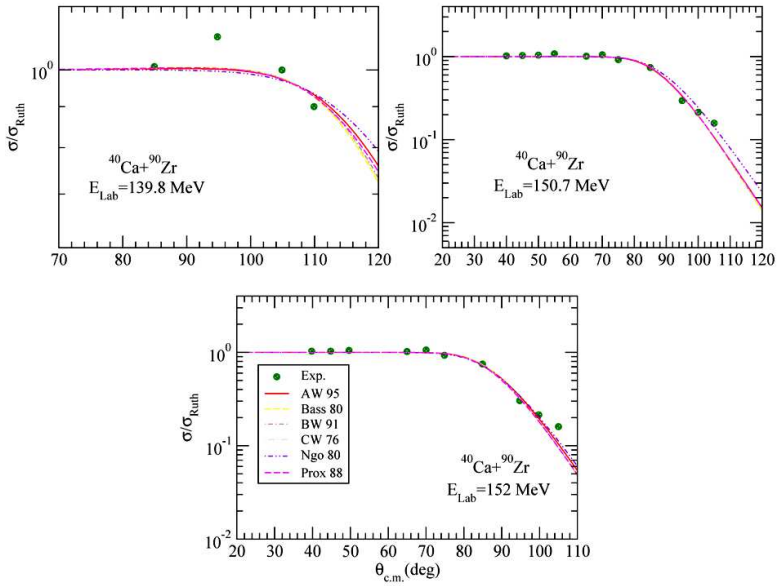

Fig. 4. The same as Fig. 2, but for the $^{40}\mathrm{Ca} + {}^{90}\mathrm{Zr}$ reaction at $E_{\mathrm{lab}} = 139.8$, 150.7, and 152 MeV. The experimental data have been taken from [4, 5]

the AW 95 potential has given slightly better results than the other potentials in describing experimental data. For 240 MeV, it has been seen that the results of CW 76 potential are slightly better than the other potential results.

The elastic-scattering cross-sections of the $^{40}\mathrm{Ca} + {}^{90}\mathrm{Zr}$ reaction at 139.8, 150.7, and 152 MeV have been shown in Fig. 4. It can be said that our results are in good agreement with the data, even though the description of experimental data

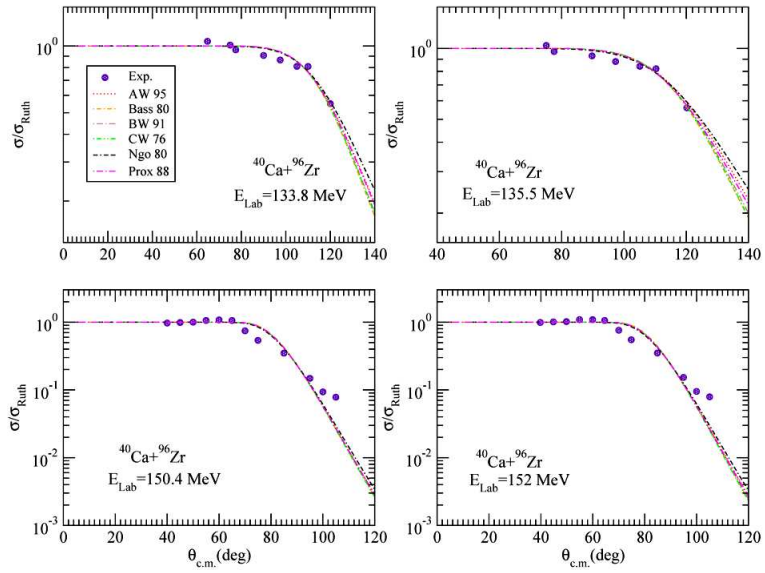

Fig. 5. The same as Fig. 2, but forthe $^{40}\mathrm{Ca} + {}^{96}\mathrm{Zr}$ reaction at $E_{\mathrm{lab}} = 133.8$, 135.5, 150.4, and 152 MeV. The experimental data have been taken from [4, 5]

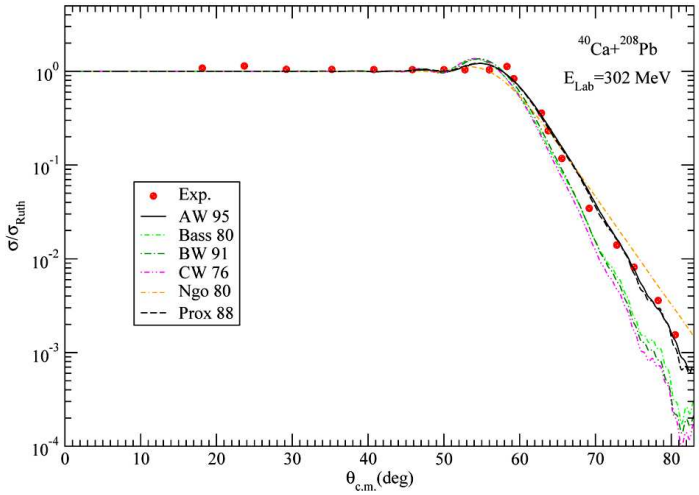

Fig. 6. The same as Fig. 2, but for the $^{40}\mathrm{Ca} + {}^{208}\mathrm{Pb}$ reaction at $E_{\mathrm{lab}} = 302$ MeV. The experimental data have been taken from [6]

is difficult at 139.8 MeV. At incident energies of 150.7 and 152 MeV, the theoretical results show very good harmony with the experimental data. Thus, we can deduce that the theoretical results with proximity potentials give a good description of the experimental data.

Another reaction investigated in this work is $^{40}\mathrm{Ca} + {}^{96}\mathrm{Zr}$. The elastic-scattering angular distributions of this reaction have been analyzed by using six various proximity potentials at 133.8, 135.5, 150.4, and 152 MeV. The theoretical results have been compared with each other, as well as with experimental data in Fig. 5. Similarly to the $^{40}\mathrm{Ca} + {}^{90}\mathrm{Zr}$ reaction, we have observed that the theoretical results have displayed a very similar behavior to each other. In addition to this, the results of the potentials are in good agreement with the experimental data. So, it can be said that the proximity potentials are quite valid in explaining the experimental data of the $^{40}\mathrm{Ca} + {}^{90}\mathrm{Zr}$ reaction.

Finally, the elastic scattering results of the $^{40}Ca + ^{208}Pb$ reaction at 302 MeV have been examined for different potentials. The theoretical results have been shown comparatively in Fig. 6. Although the results of Bass 80, BW 91, and CW 76 potentials are very close to each other, the harmony with the experimental data is poor. It has been observed that the results for AW 95 and Prox 88 potentials are very compatible with each other and are in very good agreement with the experimental data. In addition to this, we can say that the results for AW 95 and Prox 88 potentials are better, than the results of the other potentials. It has been seen that different alternative potentials could be used for the analysis of this reaction.

4. Summary

In the present work, for the first time, we have investigated the effect of six different nuclear potentials on the elastic cross-sections of ^{40}Ca scattered on ^{32}S, ^{40}Ca, ^{90}Zr, ^{96}Zr, and ^{208}Pb at various incident energies. For this purpose, we have calculated the elastic-scattering angular distributions for all the potentials and reactions and have compared our results with each other and the experimental data. We have observed that some potentials are in very good agreement with the data, and some potentials are insufficient to describe the experimental data. In this context, we have realized that the results of AW 95 potential are slightly better than the results of the other potentials. As a result of this, we can say that the theoretical results depend on the shape of a nuclear potential evaluated in the optical model analysis. Additionally, we have deduced that the proximity potentials can be applied as alternative potentials in determining the elastic-scattering data of the $^{40}Ca + ^{32}S$, $^{40}Ca + ^{40}Ca$, $^{40}Ca + ^{90}Zr$, $^{40}Ca + ^{96}Zr$, and $^{40}Ca + ^{208}Pb$ reactions. We consider that it would be beneficial and interesting in explaining different nucleus-nucleus interactions.

The author would like to thank the referee for valuable comments.

1. R.A. Broglia, A. Winther. *Heavy Ions Reactions.* (Addison-Wesley, 1991).
2. A. Baeza, B. Bilwes, R. Bilwes, J. Díazi, J.L. Ferrero. Energy-dependent renormalization coefficients of folding-model description of $^{32}S + ^{40}Ca$ elastic scattering. *Nucl. Phys. A* **419**, 412 (1984).
3. H. Doubre, J.C. Jacmart, E. Plagnol, N. Poffé, M. Riou, J.C. Roynette. Elastic scattering of ^{40}Ca by ^{40}Ca. *Phys. Rev. C* **15**, 693 (1977).
4. G. Montagnoli, S. Beghini, F. Scarlassara, A.M. Stefanini, L. Corradi, C.J. Lin, G. Pollarolo, A. Winther. Transfer reactions and sub-barrier fusion in $^{40}Ca + ^{90,96}Zr$. *Eur. Phys. J. A* **15**, 351 (2002).
5. G. Montagnoli, S. Beghini, F. Scarlassara, G.F. Segato, L. Corradi, C.J. Lin, A.M. Stefanini. Multinucleon transfer reactions of $^{40}Ca + ^{90,96}Zr$. *J. Phys. G: Nucl. Part. Phys.* **23**, 1431 (1997).
6. Yu. Ts. Oganessian, Yu.E. Penionzhkevich, V.I. Man'ko, V.N. Polyansky. Elastic scattering of ^{40}Ca and ^{48}Ca by ^{208}Pb nuclei. *Nucl. Phys. A* **303**, 259 (1978).
7. T. Izumoto, S. Krewald, A. Faessler. Nuclear matter approach to the heavy-ion optical potential: (II). Imaginary part. *Nucl. Phys. A* **357**, 471 (1981).
8. W. Reisdorf. Heavy-ion reactions close to the Coulomb barrier. *J. Phys. G, Nucl. Part. Phys.* **20**, 1297 (1994).
9. A. Winther. Dissipation, polarization and fluctuation in grazing heavy-ion collisions and the boundary to the chaotic regime. *Nucl. Phys. A* **594**, 203 (1995).
10. P.R. Christensen, A. Winther. The evidence of the ion-ion potentials from heavy ion elastic scattering. *Phys. Lett. B* **65**, 19 (1976).
11. H. Ngô, Ch. Ngô. Calculation of the real part of the interaction potential between two heavy ions in the sudden approximation. *Nucl. Phys. A* **348**, 140 (1980).
12. J. Błocki, J. Randrup, W.J. Świątecki, C.F. Tsang. Proximity forces. *Ann. Phys. (NY)* **105**, 427 (1977).
13. I.J. Thompson. Coupled reaction channels calculations in nuclear physics. *Computer Phys. Rep.* **7**, 167 (1988).
14. G.L. Zhang, Y.J. Yao, M.F. Guo, M. Pan, G.X. Zhang, X.X. Liu. Comparative studies for different proximity potentials applied to large cluster radioactivity of nuclei. *Nucl. Phys. A* **951**, 86 (2016).
15. R. Bass. Nucleus-nucleus potential deduced from experimental fusion cross sections. *Phys. Rev. Lett.* **39**, 265 (1977).
16. I. Dutt, R.K. Puri. Comparison of different proximity potentials for asymmetric colliding nuclei. *Phys. Rev. C* **81**, 064609 (2010).

Received 02.07.18

М. Айгун

ПОРІВНЯННЯ ПОТЕНЦІАЛІВ БЛИЗЬКОСТІ В АНАЛІЗІ ПЕРЕРІЗІВ ПРУЖНОГО РОЗСІЯННЯ ВАЖКИХ ІОНІВ

Р е з ю м е

Побудова альтернативних ядерних потенціалів дуже важлива для пояснення реакцій як з важкими, так і з легкими іонами. Ми вперше виконали повний аналіз шести різних потенціалів близькості ([1, 9–12, 15]). Для визначення придатності потенціалів розраховані кутові розподіли для пружного розсіювання ^{40}Ca на мішенях з різними ядрами від ^{32}S до ^{208}Pb в рамках оптичної моделі. Проведено порівняння результатів з даними експериментів. Обговорюються відмінність і схожість потенціалів і запропоновані деякі альтернативні потенціали.